





Article

Enhancement of Dopamine Electrochemical Detection with Manganese Doped Crystalline Copper Oxide

Simona Guțoiu, Florina Pogăcean *, Lidia Măgerușan , Maria Olimpia Miclăuș , Oana Grad , Ioan-Ovidiu Pană and Stela Pruneanu * 

National Institute for Research and Development of Isotopic and Molecular Technologies, 67-103 Donat Street, 400293 Cluj-Napoca, Romania; simona.gutoiu@itim-cj.ro (S.G.); lidia.magerusan@itim-cj.ro (L.M.); maria.miclaus@itim-cj.ro (M.O.M.); oana.grad@itim-cj.ro (O.G.); ovidiu.pana@itim-cj.ro (I.-O.P.)

* Correspondence: florina.pogacean@itim-cj.ro (F.P.); stela.pruneanu@itim-cj.ro (S.P.)

Abstract: Manganese doped crystalline copper oxide (CuO:Mn) and undoped CuO were prepared at room temperature by the hydrothermal method. The complete physico-chemical characterization of the materials was performed using X-ray diffraction (XRD), transmission/scanning electron microscopy (TEM/SEM), and X-ray photoelectron spectroscopy (XPS). Furthermore, their analytical applicability was tested in electrochemical experiments for a dopamine assay. According to the morphological investigation, the materials had a flat structure with nearly straight edges. The XRD analysis proved the formation of the CuO phase with good crystallinity, while the Mn doping was determined by XPS to be around 1 at.%. Under optimized conditions, at pH 5.0, the CuO:Mn modified electrode (CuO:Mn/SPE) showed a high signal for dopamine oxidation, with a linear response in the 0.1–1 μM and 1–100 μM ranges and a low limit of detection of 30.3 nM. Five times higher sensitivity for manganese doped copper oxide in comparison with the undoped sample was achieved. The applicability of the developed CuO:Mn/SPE electrode was also tested in a commercially available pharmaceutical drug with good results, suggesting that the developed sensor has promising biomedical application potential.

Keywords: CuO:Mn/SPE electrode; dopamine sensing; SPE modified electrode



Citation: Guțoiu, S.; Pogăcean, F.; Măgerușan, L.; Miclăuș, M.O.; Grad, O.; Pană, I.-O.; Pruneanu, S. Enhancement of Dopamine Electrochemical Detection with Manganese Doped Crystalline Copper Oxide. *Coatings* **2023**, *13*, 1014. <https://doi.org/10.3390/coatings13061014>

Academic Editor: Arūnas Ramanavičius

Received: 25 April 2023

Revised: 24 May 2023

Accepted: 26 May 2023

Published: 30 May 2023



Copyright: © 2023 by the authors. Licensee MDPI, Basel, Switzerland. This article is an open access article distributed under the terms and conditions of the Creative Commons Attribution (CC BY) license (<https://creativecommons.org/licenses/by/4.0/>).

1. Introduction

Dopamine (DA)—also known as 3,4-dihydroxytyramine or the ‘feel-good’ hormone—is an endogenous catecholamine neurotransmitter that plays a crucial role in general mental and physical health, being involved in the brain’s reward/pleasure systems; regulation of peripheral organs and motor coordination; gastrointestinal motility; blood pressure maintenance; mood management; hormone release; memory and attention; as well as in immunoregulation [1–4]. For a healthy person, the DA concentration in the extracellular fluid is in the range of 0.01–1 μM [5]. Abnormal dopamine levels have been associated with various neurological and physical disorders, including Parkinson’s disease, schizophrenia, stress, ADHD, HIV infection, obesity, depression, hallucination, addiction, cardiotoxicity, hypertension, and heart failure [6–9]. Therefore, the development of techniques for the accurate and sensitive detection of dopamine is of significant interest in both clinical and research settings not only to regulate drug treatment, but also to facilitate the early diagnosis of diseases. Until now, various analytical tools have been developed and employed for dopamine assay including biochemical techniques—such as enzyme linked immuno-sorbent assay ELISA [10]; high-performance liquid chromatography—HPLC or reverse-phase HPLC [11,12]; spectrometric and spectrophotometric methods [13,14]; and capillary electrophoresis [15]. Since it was proved that dopamine electro-oxidation at conventional electrodes can be easily achieved [16]; the electrochemical approach gains a lot of popularity compared to the traditional detection methods, since electrochemical

techniques are straightforward to use, generate a rapid response with minimal expense and high selectivity, and do not necessitate bulky machinery or highly trained personnel [17]. Moreover, dopamine electrochemical detection has proven to be a powerful tool for understanding the complex mechanisms underlying dopamine-related disorders and developing novel therapeutic approaches. However, there are some serious drawbacks in dopamine electrochemical detection related to electrode sensitivity and selectivity. In order to surmount these challenges, a variety of sensing materials have been developed and applied at the electrode surface including antibodies, enzymes, or aptamers [18–21]; molecularly imprinted polymers [22,23]; or nanomaterials [24–29]. In the last decade, electrochemical biosensors have been widely used and seen as a major advancement in real-time monitoring of catecholamine neurotransmitters [30]. Decarli et al. [31] report the usage of imidazolium zwitterionic surfactants in the development of new biosensors for DA determination while Pimpilova et al. [32] results present sensitive DA detection based on laccase immobilized on glassy carbon electrode modified with nanoporous gold. Alvarez and Ferapontova [33] developed an RNA-based dopamine aptasensor, which has a sub-micromolar detection limit. In addition, recent reports have shown the development of different catecholamine biosensors using enzymes such as PQQ-dependent glucose dehydrogenase [34] and polyphenol oxidases [35]. Furthermore, Winiarski and his collaborators managed to reuse waste from the steel industry as a sustainable electrode modifier material for the electrochemical monitoring of different neurotransmitters [36].

Among various electrode modifiers, metal oxide nanoparticles and nanostructures are advantageous as dopamine sensing materials—[37–41], owing to their high conductivity, superior electrocatalytic properties and biocompatibility [42].

Copper (II) oxide (CuO) has been widely used for a variety of applications such as electrochemical sensors, gas sensors, solar energy, batteries, and green catalysts—[43–45] due to its p-type semiconductor properties and band gap of 1.2 to 2.2 eV. Based on this metal oxide, various platforms were synthesized and used as electrochemical sensors for the detection of H₂O₂ [46–49], glucose [50–52], dopamine [53,54], cysteine [55], L-tyrosine [56], fructose [57], acetaminophen, and caffeine [58].

Nowadays, the fabrication of materials with tunable magnetic, photocatalytic, photovoltaic, and electrochemical properties are considered one of the most scientific challenges [59–61]. Special attention was accorded to doping with different transition elements: Zn [62], In [63], Mn [64], Fe [65], and Ni [66] of CuO in order to improve its physical and chemical performances. Among the dopants, manganese was chosen due to its main oxidation states, Mn²⁺ and Mn³⁺, and its ionic radii that match with Cu²⁺ ionic radii. Herein, we presented a facile low-cost hydrothermal method for the synthesis of pure manganese doped copper oxide material, with application in electrochemistry. Our aim was to test the capacity of Mn doped CuO hybrid material as DA sensing material. According to our study, performed on an available pharmaceutical drug solution, the screen printed CuO:Mn modified electrode has an excellent ability in the determination of dopamine in a real sample. To the best of our knowledge, studies which report the influence of Mn dopant on dopamine sensing properties of CuO were not published.

2. Materials and Methods

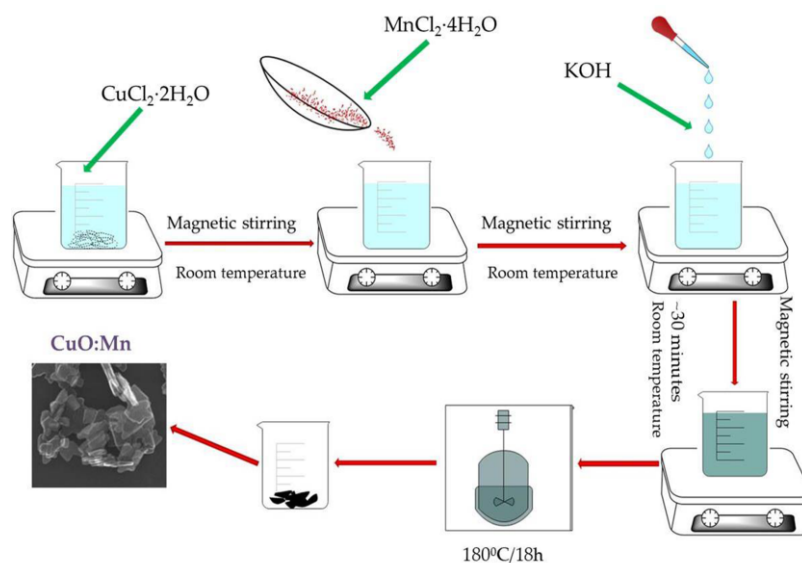
2.1. Materials

All reagents were used without further purification. Copper (II) chloride dihydrate, 99% purity, was purchased from Alfa Aesar (Kandel, Germany) manganese (II) chloride tetrahydrate, ≥98% purity, was purchased from Sigma Aldrich (Darmstadt, Germany), KOH, 99.4% purity, was purchased from Lach:ner (Továrni, Czech Republic) and dopamine hydrochloride (99%) was purchased from Alfa Aesar (Kandel, Germany).

2.2. Synthesis of Copper Oxide (CuO) and Manganese Doped Copper Oxide (CuO:Mn) Samples

Copper oxide and manganese doped copper oxide were prepared, applying the slightly modified method indicated by A. Khalid et al. [67]. Hence, CuCl₂·2H₂O, MnCl₂·4H₂O, and

KOH were used as precursors for the manganese doped sample. First, an aqueous solution was obtained by dissolving 1.7 g of copper chloride dihydrate in 20 mL deionized water. The amount of manganese chloride tetrahydrate was calculated in order to obtain 1 at.% Mn. The manganese precursor was added to the first solution. A mixture of 1.35 g KOH and 20 mL deionized water was prepared separately and added dropwise over the first solution. All procedures were performed at room temperature under continuous magnetic stirring. After about 30 min, the aquamarine color of the obtained precipitate changes to dark brown. The whole mixture was transferred to a Teflon autoclave and left for 18 h at 180 °C in the oven. The black Mn doped CuO particles obtained were washed with deionized water and dried in the oven at 65 °C overnight. In Scheme 1, the full procedure for obtaining the CuO:Mn material is described. For the CuO sample, the same steps were performed without adding the manganese precursor.



Scheme 1. Schematic illustration showing chemical synthesis of manganese doped copper oxide.

2.3. Characterization Methods

The crystalline structure of prepared samples was examined by X-ray diffraction using a Rigaku-Smart Lab automated multipurpose X-ray diffractometer. The equipment was equipped with a high-accuracy θ - θ goniometer and works with $\text{CuK}\alpha$ radiation ($\lambda = 1.54060 \text{ \AA}$) in reflection mode.

The morphological characterization was performed through scanning transmission electron microscopy (STEM) using a Hitachi HD2700 electron microscope, equipped with a cold field emission gun operating at 200 kV.

The qualitative and quantitative sample compositions were investigated using X-ray photoelectron spectroscopy (XPS) assisted by Ar ions etching.

The XPS spectra were recorded using a SPECS spectrometer working with a monochromatized Mg anode (1253.6 eV) as the X-ray source. The spectra were recorded with an energy pass of 30 eV, at a dwell time of 0.2 s and a step size of 0.1 eV. The sample powders from an alcohol suspension were deposited on a tungsten sample holder and dried at room temperature. In order to avoid the artificial reduction of the different oxidation states of elements under the Ar ions beam, the etching was performed by using ions accelerated at a maximum voltage of 1000 V with a filament current of 10 mA. The etching was performed until the areas of various core-levels remained unchanged. Thus, the weight of the surface states was brought to real values in comparison with the states inside the nanoparticles. At this stage, the sample is susceptible to quantitative analysis. The quantification of the various peaks was made through CASA software. All the integral intensities were calibrated by using the relative sensitivities, transmission, and electronic mean free path factors, as given in the CASA software database. Adventitious carbon, at 284.6 eV, was used for binding

energies calibration. A Shirley background was considered for the quantification of the XPS spectra.

Cyclic voltammetry (CV), square wave voltammetry (SWV) and electrochemical impedance spectroscopy (EIS) measurements were recorded with a potentiostat/galvanostat instrument (AUTOLAB-302N; Utrecht; The Netherlands) coupled with a computer and a three-electrode cell: working electrode (bare and modified SPE), and a large area (2 cm^2) platinum counter electrode and Ag/AgCl (KCl saturated) reference electrode. EIS measurements were recorded between $0.01\text{--}10^5$ Hz, in solution containing 10^{-4} M dopamine (pH 5.0). The experimental data were fitted with NOVA 1.11 software.

2.4. Modification of Screen Printed Electrodes (CuO/SPE and CuO:Mn/SPE)

In order to test the electrochemical properties of CuO and CuO:Mn materials, they were first dispersed by ultrasound in N,N-dimethylformamide (DMF), at a concentration of 2 mg/mL. Next, two screen-printed electrodes (SPE-Metrohm (DRP-110)) were modified with 10 μL of colloidal suspension of each sample and were allowed to dry at room temperature for 24 h. The modified electrodes were correspondingly denoted CuO/SPE and CuO:Mn/SPE. The interaction between CuO/CuO:Mn particles and the graphite surface was not only physical interaction, due to the high porosity of the working electrode, but also chemical interaction through van der Waals forces. The amount of deposited oxide particles was reproducible from one run to another (RSD < 7%; RSD was evaluated from a dopamine oxidation peak from 5 different modified electrodes).

The DRP-110 electrodes have the following characteristics: ceramic substrate: $L33 \times W10 \times H0.5$ mm; electrical contacts: silver. The electrochemical cell consists of a working electrode (carbon—4 mm diameter); auxiliary electrode (carbon), and reference electrode (silver). Optical images of SPE electrodes can be seen in Figure S1.

3. Results and Discussion

3.1. Characterization of CuO and CuO:Mn Samples

3.1.1. Structural Characterization

The crystal structures and phase information of CuO and CuO:Mn were characterized by X-ray diffraction (XRD). The results are presented in Figure 1. The crystalline phase identified in the samples was similar to CuO corresponding to the PDF-2 database ref. cod 100-089-5899 (space group Cc(9)- monoclinic). Due to the small amount of Mn (~1 at.%) added in reaction to obtain the CuO:Mn doped sample, XRD cannot detect such a small amount, so the diffraction peaks of CuO:Mn does not suffer structural changes detectable by XRD. The typical diffraction peaks correspond to the (110), (002), (111), (-112), (-202), (112), (021), (202), (022), (113), (220), (-312), (221), and (-204) crystal planes of copper oxide.

The crystallite mean size was calculated from the full width at half maximum (FWHM) for (1 1 2) reflections ($2\theta = 48.75^\circ$) by using the Scherrer equation. The mean size of the crystallites obtained for the CuO phase is 48.43 nm while in the case of the CuO:Mn sample, the crystallites have an almost half value of 27.02 nm. Generally, the narrower the diffraction peak the larger the mean crystallite size. Thus, in the case of large CuO crystallites, the maxima corresponding to (310) and (113) planes are narrow and are better resolved. In the case of the CuO:Mn phase, with smaller crystallites, the mentioned neighboring reflections are partially superposed.

3.1.2. Morphological Characterization

The morphologies of CuO and CuO:Mn samples were examined by TEM (Figure 2a,c) and SEM techniques (Figure 2b,d). For both samples, it can be observed that the obtained particles have the size in the micrometer range, but the size distribution is not homogeneous. At the same time, in the case of the non-doped sample, particles with a large size predominate, while for the doped sample, smaller particles prevail. The particles of CuO material have more elongated shapes than the particles of doped material. After determining the degree of crystallinity by XRD, a good agreement was found between the

crystallinity of each sample and its particle sizes. The different morphology of the samples may be attributed to manganese which replaces copper ions in the CuO lattice. Most of those particles have flattened faces and irregular shapes with nearly straight edges which are more pronounced in the case of doped samples.

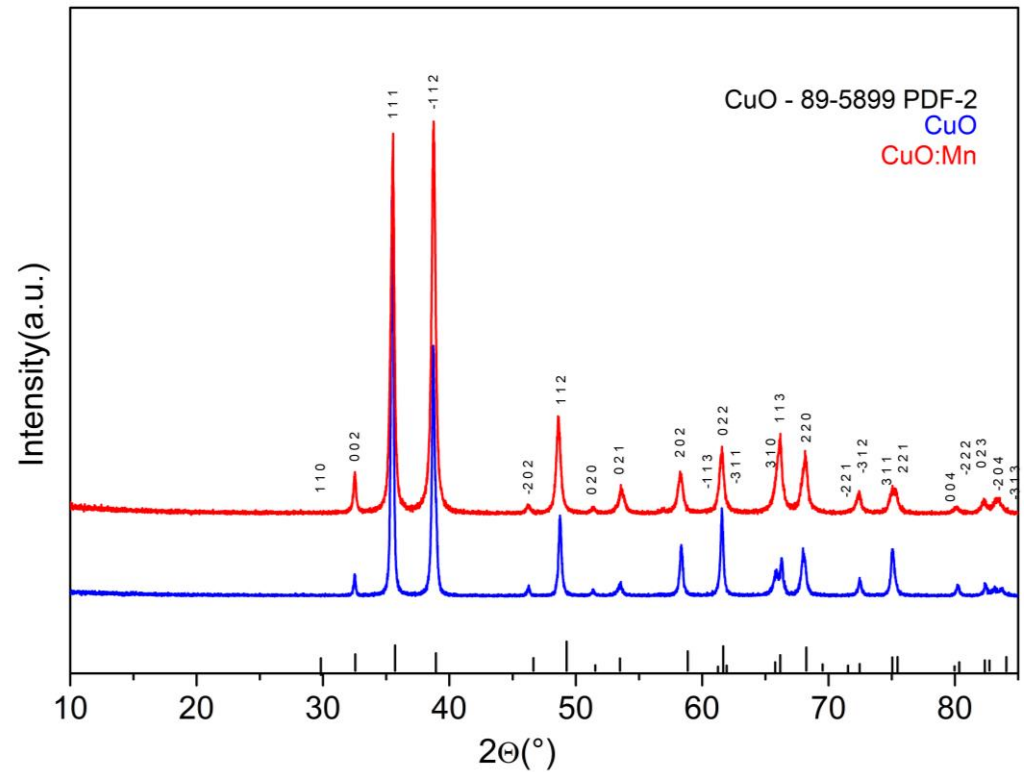


Figure 1. XRD patterns registered for CuO (blue) and CuO:Mn (red) materials.

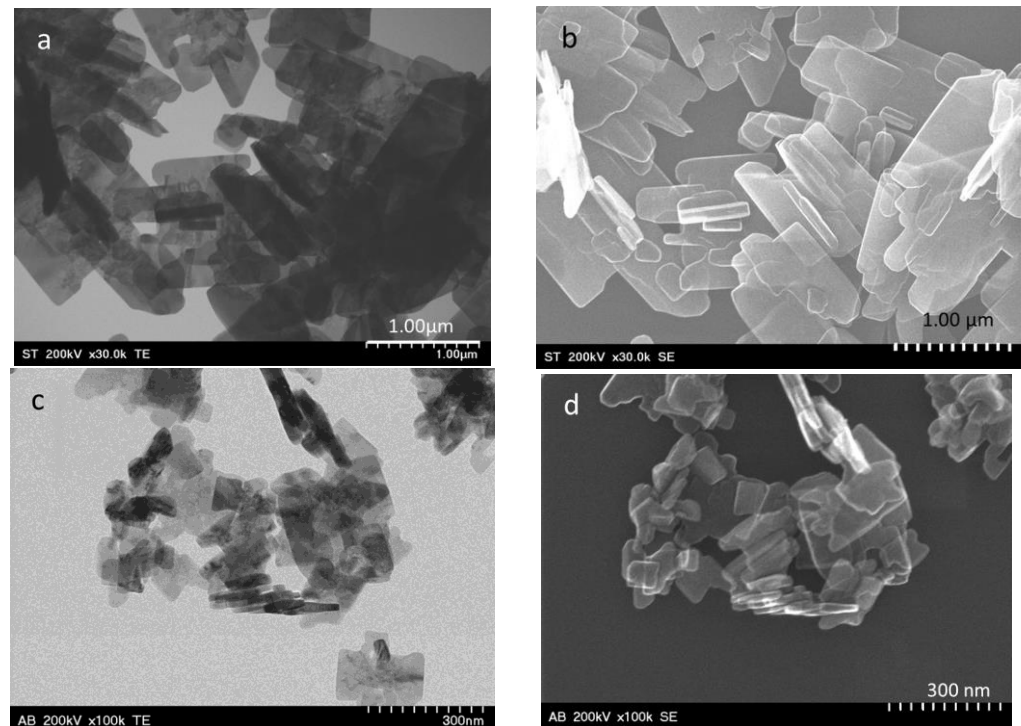


Figure 2. TEM and SEM micrographs for CuO (a,b) and CuO:Mn (c,d) materials.

3.1.3. Qualitative and Quantitative Characterization of CuO:Mn

The XPS technique was used to further check the sample composition. The XPS technique, although it is a surface technique, when it is used in the case of nanostructured materials and is associated with Ar ion etching, allows a quantitative analysis (including the doping level) of the composition of the nanostructures [68]. This is due to the fact that Ar ion etching smooths the sample, made up of agglomerated particles. A very large number of particles of the ensemble will be sectioned, each at different depths, and surface effects are thus compensated. At this stage the XPS core levels intensities reflect the sample composition.

Evidently, this procedure is not valid for bulk materials. Comparative C 1 s core-level spectra before and after different etching stages are inserted in the Supporting Material as Figure S2. No shifts of C 1 s peak position, used for calibration, were observed here. The XPS recorded spectra of the Cu 2p core-level doublet together with the corresponding deconvolutions and fitted curves are shown in Figure 3. There are two copper positions (two doublets): the main spin-orbit doublet peaks, corresponding to Cu²⁺ inside the particles, at 933.8 and 953.8 eV, and a doublet, positioned by 2.5 eV at higher binding energies (BE), which corresponds to the copper surface states at 936.4 and 956.4 eV, respectively. At much higher energies, two shake-up satellite features appear in spectra around 942.3 and 944.5 eV for (3/2) peaks and at 963.2 and 963.8 eV for (1/2) peaks, respectively. It is the signature of the presence of the Cu²⁺ state [69]. The restrictions used to fit the Cu 2p XPS spectra refer to the relation between areas of the two components, $A_{1/2} = A_{3/2}/2$, and to the doublet energy separation, which was adjusted between 11.9 and 12.0 eV. The ratios between (1/2) and (3/2) linewidths were set between 1 and 1.1.

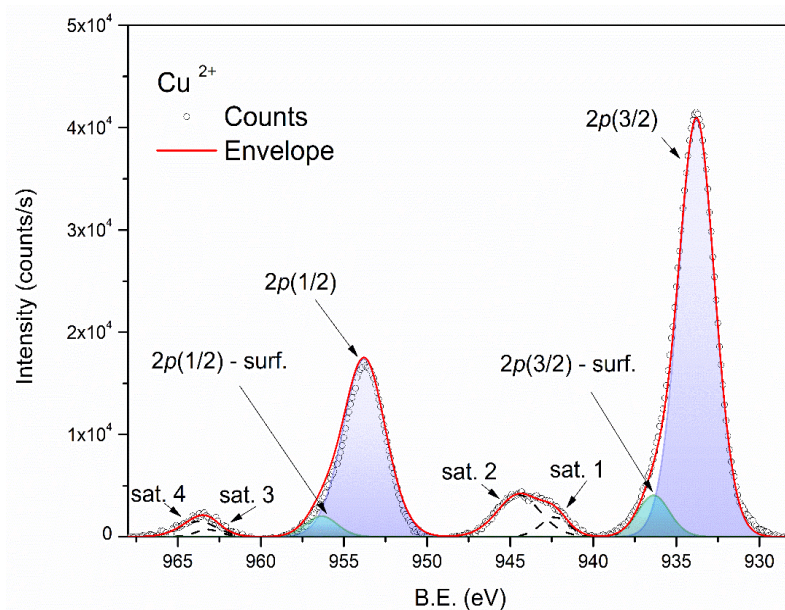


Figure 3. XPS recorded spectrum of Cu 2p core-level of CuO:Mn sample together with the corresponding deconvolutions and fitted curves. Peaks labeled 2p (1/2)-surf and 2p (3/2)-surf correspond to the copper surface states. Four shake up satellites are also presented in the spectra.

There are no major differences between the positions of the lines in the Cu 2p core-levels spectra of CuO:Mn and CuO, respectively. The latter, together with the survey spectrum of CuO, are presented in Figures S3 and, respectively, S4 from Supporting Materials. What can be observed in the case of undoped CuO is a higher intensity of the peaks corresponding to the surface states of Cu²⁺ with OH termination. From the spectrum in Figure S4 it can be observed that there are no detectable amounts of Cl remaining from the precursor.

In addition, the presence of the CuLMM Auger peak, at the kinetic energy of 917.7 eV (Figure 4), is a characteristic of the existence of Cu²⁺ states in the sample. The line shape is also specific to this oxidation state [70].

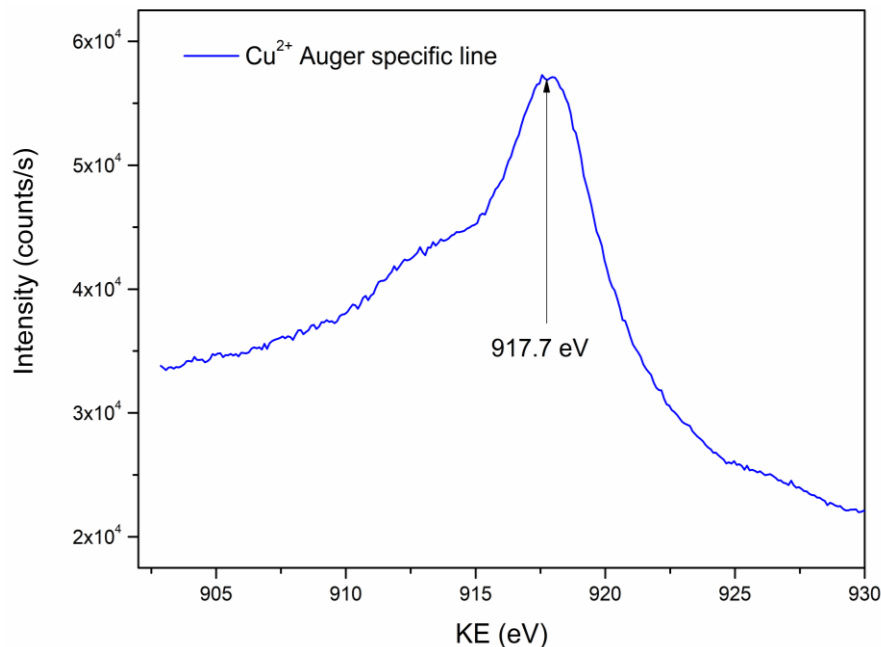


Figure 4. The CuLMM Auger spectra recorded for Cu²⁺.

The XPS spectrum corresponding to the O 1s core level is shown in Figure 5. Three oxygen positions can be noted here. The most intense peak corresponds to the oxygen inside the nanoparticles (lattice oxygen), while the two others at higher binding energies are related to the presence of surface hydroxyl groups formed at oxygen terminated surfaces (~534.4 eV) and hydroxyl groups (~533.5 eV) attached to the Cu terminated surfaces. They are mainly due to the aqueous solutions used in preparation [71,72].

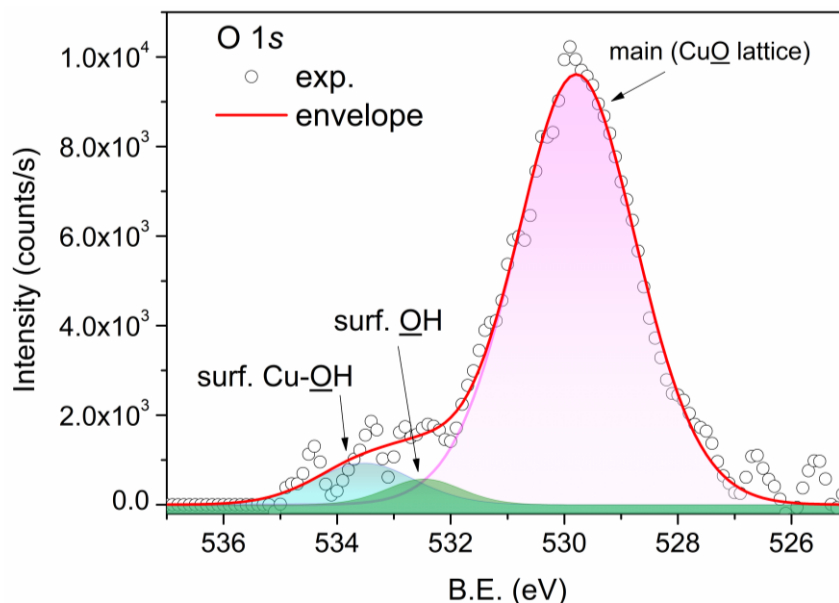


Figure 5. XPS recorded spectrum of O 1s core level of CuO:Mn sample together with the corresponding deconvolutions and fitted curves.

The ratio between the areas corresponding to Cu atoms and those corresponding to O1s is noted to be around 1.026, which confirms the stoichiometry of the particles.

Features corresponding to the dopant manganese (Mn 2p core-level) are presented in Figure 6. The corresponding doublet positions are 640.6 (3/2) and 651.9 (1/2) eV with a spin orbit splitting of 11.2 eV. These values are consistent with the Mn²⁺ state. Based on the normalized areas of the XPS peaks, the concentration of manganese ions in the sample was found to be 1.2 ± 0.5 % in good agreement with its nominal value.

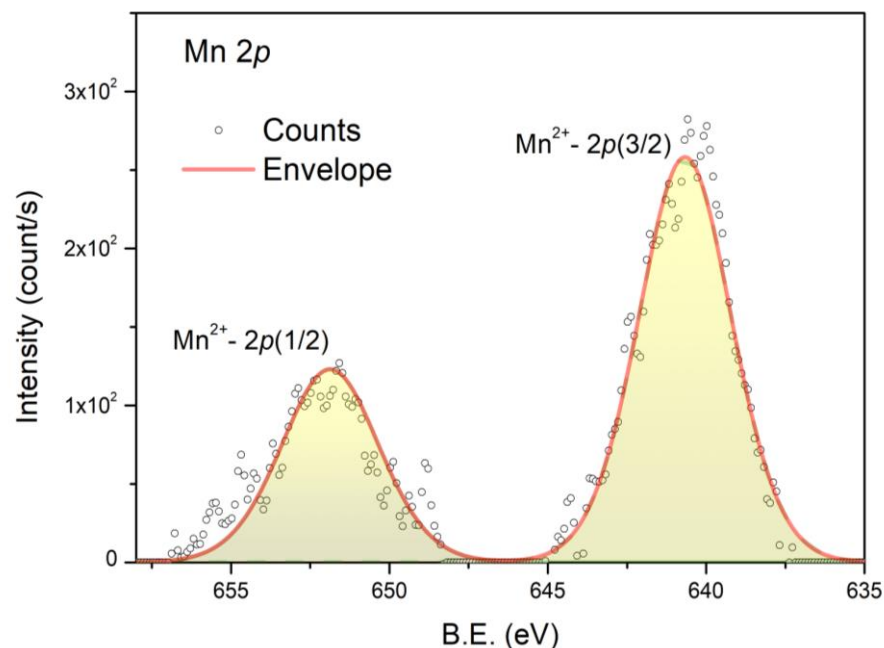


Figure 6. XPS recorded spectrum of Mn 2p core-level doublet of manganese dopant together with corresponding deconvolutions and fitted curves.

Table S1 summarizes the binding energies, line widths and core-level areas of Cu 2p, O1s and Mn 2p. The normalized areas presented in the last column are proportional to the number of atoms in the respective species.

3.2. Electrochemical Detection of Dopamine

Before starting the experiments for dopamine detection with bare and SPE modified electrodes, the active areas of electrodes were determined using the Randles–Ševčík equation. Thus, cyclic voltammograms were recorded with different scanning rates (2–100 mV/s) in solution containing 10^{−3} M potassium hexacyanoferrate (II) and 0.2 M KCl supporting electrolyte. Next, the anodic peak current (*I*_{pa}) was represented *versus* the square root of the scan rate (*v*^{1/2}) (for exemplification, the results for the bare SPE and CuO:Mn/SPE are shown in the Supporting Material, Figures S5a,b and S6a,b, respectively). From the slope of each plot, the active area of the corresponding electrode was determined to be: A = 0.1 cm² (bare SPE); A = 0.057 cm² (CuO/SPE); and A = 0.084 cm² (CuO:Mn/SPE). The decrease of the SPE active area after modification with CuO or CuO:Mn particles may be explained by the decrease in the electrode's porosity and consequently its roughness.

Next, the pH effect on the DA oxidation signal was thoroughly investigated. In Figure 7, the CVs recorded with CuO:Mn/SPE in 10^{−4} M dopamine solutions having various pH values (3.6–8.0) are shown. In all cases, a well-defined oxidation peak was observed, accompanied by a reduction peak of lower intensity. Although the peak potential separation (ΔE_p) was generally small (~0.35 V in acidic solutions; ~0.5 V in neutral and basic solutions) the *I*_{pa}/*I*_{pc} ratio was higher than 1, so the process may be regarded as quasi-reversible. In this case the rate of electron transfer is comparable to that of mass transport. The CV curves shown in Figure 7 correspond to the first scan for each pH

solution. As expected, upon increasing the number of scans, a small variation in the oxidation/reduction signals was observed, due to the adsorption of the oxidation product on the electrode surface (See Figure S7).

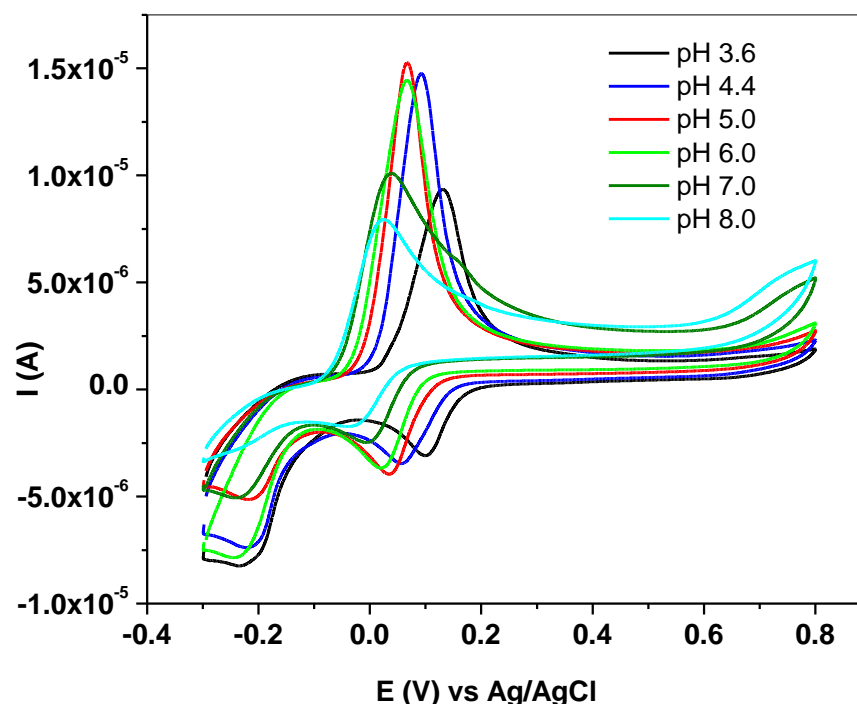


Figure 7. CVs recorded with CuO:Mn/SPE in 10^{-4} M dopamine solutions having various pHs (3.6–8.0); 10 mV/s scan rate (acetate buffers were used for pH 3.6–pH 5.0 solutions and phosphate buffer saline were used for pH 6.0–pH 8.0 solutions).

Additional information can be obtained by looking at the plots of anodic peak current (I_{pa}) and peak potential (E_{pa}) versus the solution pH (Figure 8a,b). In case of the peak current, one can see that it gradually increased with pH up to the value of pH 5.0, and then strongly decreased. Therefore, the optimal pH electrolyte solution was selected to be pH 5.0 acetate buffer.

In the case of the anodic peak potential, its variation with the buffer pH follows the linear regression equation: $E_{pa} = 0.19 - 0.022 \times \text{pH}$ ($R^2 = 0.986$). The slope is equal to 0.022 V/pH which is very close to half of the Nernstian value (0.057 V/pH at 25 °C), indicating that the H^+/n ratio is equal to 1/2. Similar results for the slopes were reported by Jayadevappa et al. [54] with electrodes modified with CuO nanoparticles. In their case, the electrodes were based on carbon paste mixed with flake- and rod-shaped CuO nanoparticles. The generally accepted mechanism for dopamine oxidation involves the transfer of $2e^-$ and $2H^+$, with its transformation into dopamine ortho-quinone.

In order to explain the small value obtained for the E_p versus pH slope, we suggest that some of the protons generated during dopamine oxidation are used to reduce the OH groups linked to CuO particles (e.g., CuOOH is reduced to Cu(OH)₂), which changes the pH around the electrode surface. These protons account for the E_p versus pH slope. The other protons are involved in the reaction with the acetate solution, to keep the pH constant at the electrode surface. Acetic acid/sodium acetate employed for the preparation of the pH 5.0 solution contains acetate ions, hydrogen ions, and un-dissociated acetic acid molecules. The acetate ions can react with H^+ ions added to solution during dopamine oxidation to produce acetic acid. In this way, the pH value at the electrode surface is maintained constant, but the corresponding protons do not influence the E_p versus pH slope.

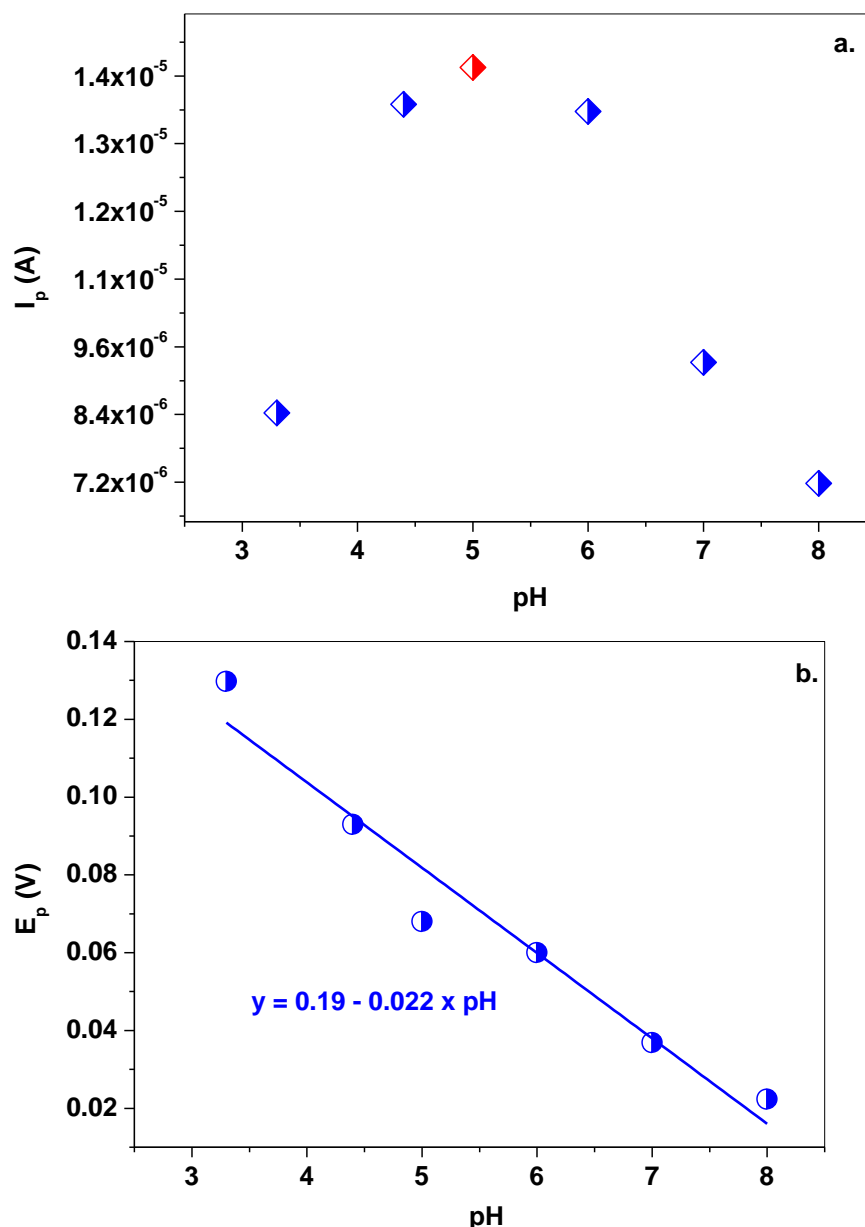


Figure 8. Variation of the anodic peak current, I_{pa} , with the pH (a); variation of the anodic peak potential, E_{pa} , with the pH (b).

Next, the effect of the scan rate on the dopamine oxidation signal was investigated by cyclic voltammetry. The CV recordings are presented in Figure S8a (Supporting Materials), where the change of the anodic and cathodic waves with the scan rate (2–550 mV/s) can be observed. By representing the corresponding peak current (I_p) versus the square root of the scan rate ($v^{1/2}$), linear plots are obtained, indicating that the electron transfer reaction between dopamine and the CuO:Mn/SPE surface is diffusion-controlled (Figure S8b). The linear regression equations, corresponding to the anodic and cathodic plots are $y = -1.77 \times 10^{-6} + 8.88 \times 10^{-5} \times v^{1/2}$ ($R^2 = 0.997$; anodic) and $y = -1.14 \times 10^{-6} - 1.63 \times 10^{-5} \times v^{1/2}$ ($R^2 = 0.989$; cathodic).

In order to evidence the electro-catalytic effect of CuO:Mn/SPE towards dopamine oxidation, SW technique was employed. This technique has the advantage of the elimination of the capacitive current; therefore, the redox signals obtained with different electrodes can be easily compared. Hence, SW voltammograms were recorded in 10^{-4} M dopamine (pH 5.0 acetate buffer) with CuO:Mn/SPE and the results are presented in comparison with

those obtained for bare SPE and CuO/SPE (Figure 9). In the case of bare SPE, the dopamine oxidation signal is low and appears at a potential of +0.175 V. After SPE modification with CuO nanoparticles, a shift in the peak potential was observed (down to +0.085 V) without the significant increase of the peak current. The CuO:Mn/SPE has the strongest electro-catalytic effect, evidenced by the further shift of the peak potential (down to +0.075 V) and the considerable increase in the peak current (five times compared to that of bare SPE or CuO/SPE). This indicates that the presence of a small amount (1 at. %) of dopant manganese in the catalyst (CuO) is useful for promoting the transfer of electrons between the dopamine molecules and SPE surface. The results are in excellent agreement with those obtained by electrochemical impedance spectroscopy (see the next paragraph).

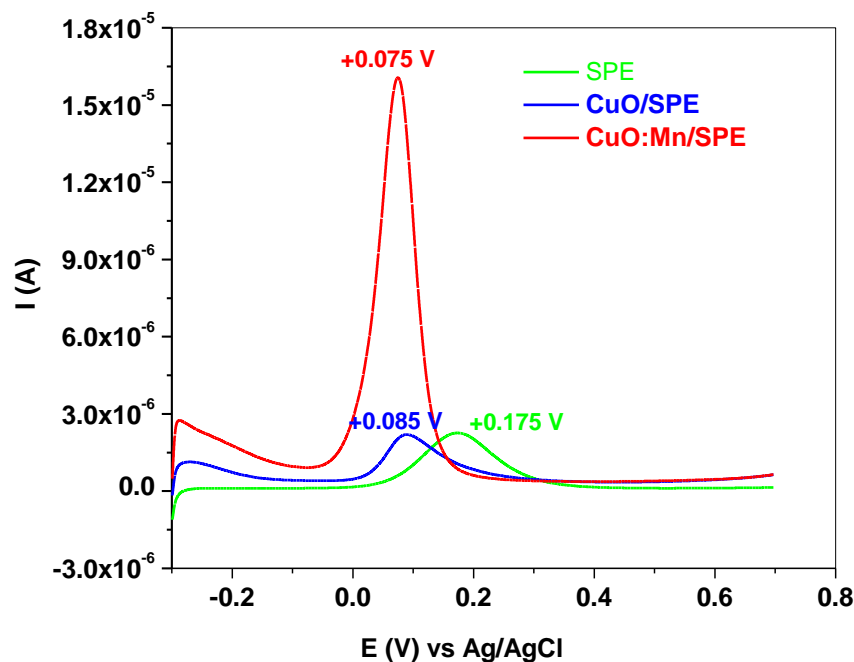


Figure 9. SW voltammograms recorded in 10^{-4} M dopamine (pH 5.0 acetate buffer) with bare SPE (green); CuO/SPE (blue) and CuO:Mn/SPE (red); 10 mV/s scan rate.

EIS is a very useful technique since it can provide information about the charge-transfer resistance (R_{ct}) of various materials. In our case, we compared the EIS spectra (represented as Nyquist plots) of bare SPE and SPE modified electrodes (CuO/SPE, respectively, CuO:Mn/SPE—Figure 10). For bare SPE, the plot reveals a large semi-circle in the high-medium frequency range which can be attributed to the charge-transfer resistance (R_{ct}) of the material followed by a straight line at low frequencies, due to the diffusion of the redox species within the double-layer and described by the Warburg impedance (W). The double-layer capacitance (C_{dl}), generally employed to describe the charging of the double-layer, was replaced in our case by a constant phase element (CPE), since it better fit the behavior of electrodes with porous morphologies. In addition, the circuit contains the solution resistance (R_s). The same electrical circuit was used to fit the data recorded with CuO/SPE and CuO:Mn/SPE (Figure S9). The R_{ct} values obtained after fitting the EIS spectra with the equivalent electrical circuit were found to be: 58 k Ω (SPE); 56 k Ω (CuO/SPE); and 208 Ω (CuO:Mn/SPE). It is interesting to mention that the addition of CuO:Mn on top of SPE significantly decreased the R_{ct} value which may be related to the fact that dopamine adsorption upon the electrode surface depends on the type of electrodes. If the EIS plots are compared, it is clear that the semicircle of CuO/SPE is more depressed than that of bare SPE, which is a good indication that electrode passivation resulting from adsorption is higher for SPE. The straight line observed for CuO:Mn/SPE, with low real and imaginary values, indicates that there is a lower amount of adsorbed material to hinder the electrochemical reactions between the diffusion layer and the electrode surface.

Consequently, the CuO:Mn particles have the ability to swiftly transfer the electrons with dopamine molecules from solution.

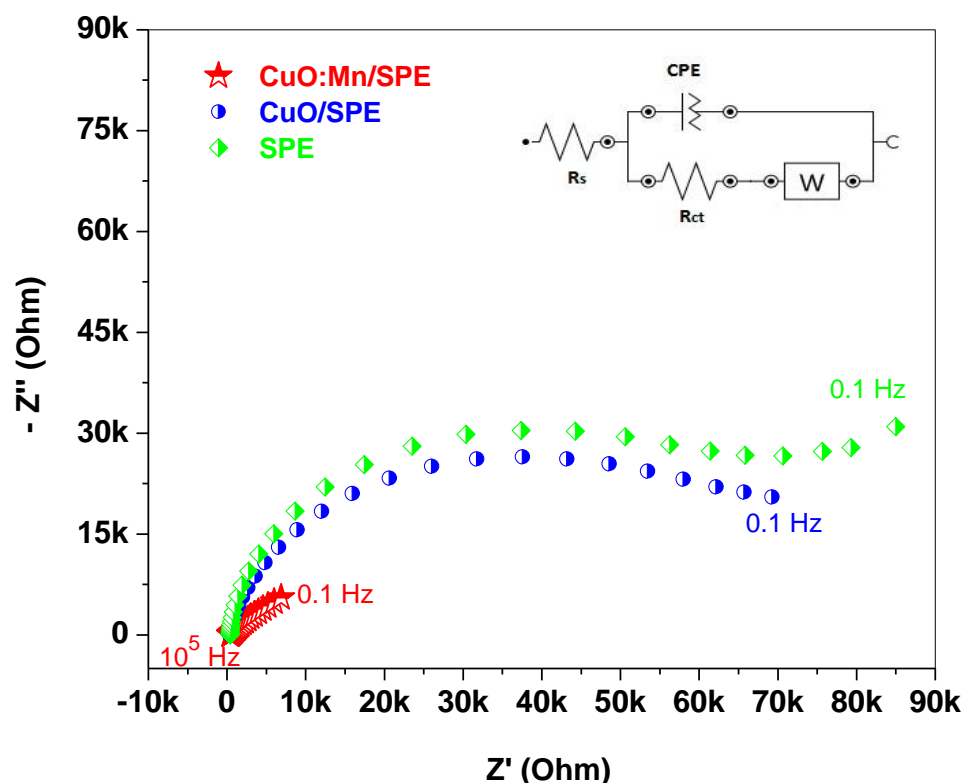


Figure 10. Nyquist plot recorded in 10^{-4} M dopamine (pH 5.0 acetate buffer) for bare SPE (green; $E_{1/2} = +0.149$ V applied potential) and modified electrodes: CuO/SPE (blue; $E_{1/2} = +0.064$ V applied potential); and CuO:Mn/SPE (red; $E_{1/2} = +0.047$ V applied potential); inset: the equivalent electrical circuit employed to fit the Nyquist plots of bare and SPE modified electrodes.

Using the determined R_{ct} values, the apparent heterogeneous electron transfer rate (k_{app}) was calculated for all electrodes based on the following equation [73]:

$$k_{app} = \frac{RT}{n^2 F^2 A R_{ct} C} \quad (1)$$

where n is the number of electrons transferred during the redox reaction ($n = 2$); F is the Faraday constant ($96,485 \text{ C mol}^{-1}$); R is the ideal gas constant ($8.314 \text{ J mol}^{-1} \text{ K}^{-1}$); T is the temperature (298 K); A is the active area of the electrode (cm^2); R_{ct} is the charge-transfer resistance obtained from the fitted Nyquist plots (Ω); C is the concentration of the redox species ($\text{mol} \cdot \text{cm}^{-3}$).

Hence, k_{app} was determined to be: $1.15 \times 10^{-4} \text{ cm/s}$ for SPE; $2.08 \times 10^{-4} \text{ cm/s}$ for CuO/SPE and $3.8 \times 10^{-2} \text{ cm/s}$ for CuO:Mn/SPE. One can see that k_{app} is two orders of magnitude higher than that corresponding to bare SPE or CuO/SPE, clearly indicating that the doping of CuO with Mn atoms highly promotes the transfer of electrons from dopamine molecules to SPE substrate.

Next, the SW technique was employed for studying the effect of dopamine concentration on the electrochemical signal obtained with different electrodes and to determine other important analytical parameters, such as linear range, limit of quantification (LOQ), limit of detection (LOD), and sensitivity. In Figure 11a,b are present the signals recorded with CuO:Mn/SPE (a) and CuO/SPE (b), within a 10^{-7} – 10^{-4} M dopamine concentration range. The signals obtained for bare SPE can be seen in Figure S10 (Supporting Materials). Marked differences between the three electrodes are observed by plotting the anodic peak current, I_{pa} , versus the dopamine concentration (C_{DA}), Figure 12.

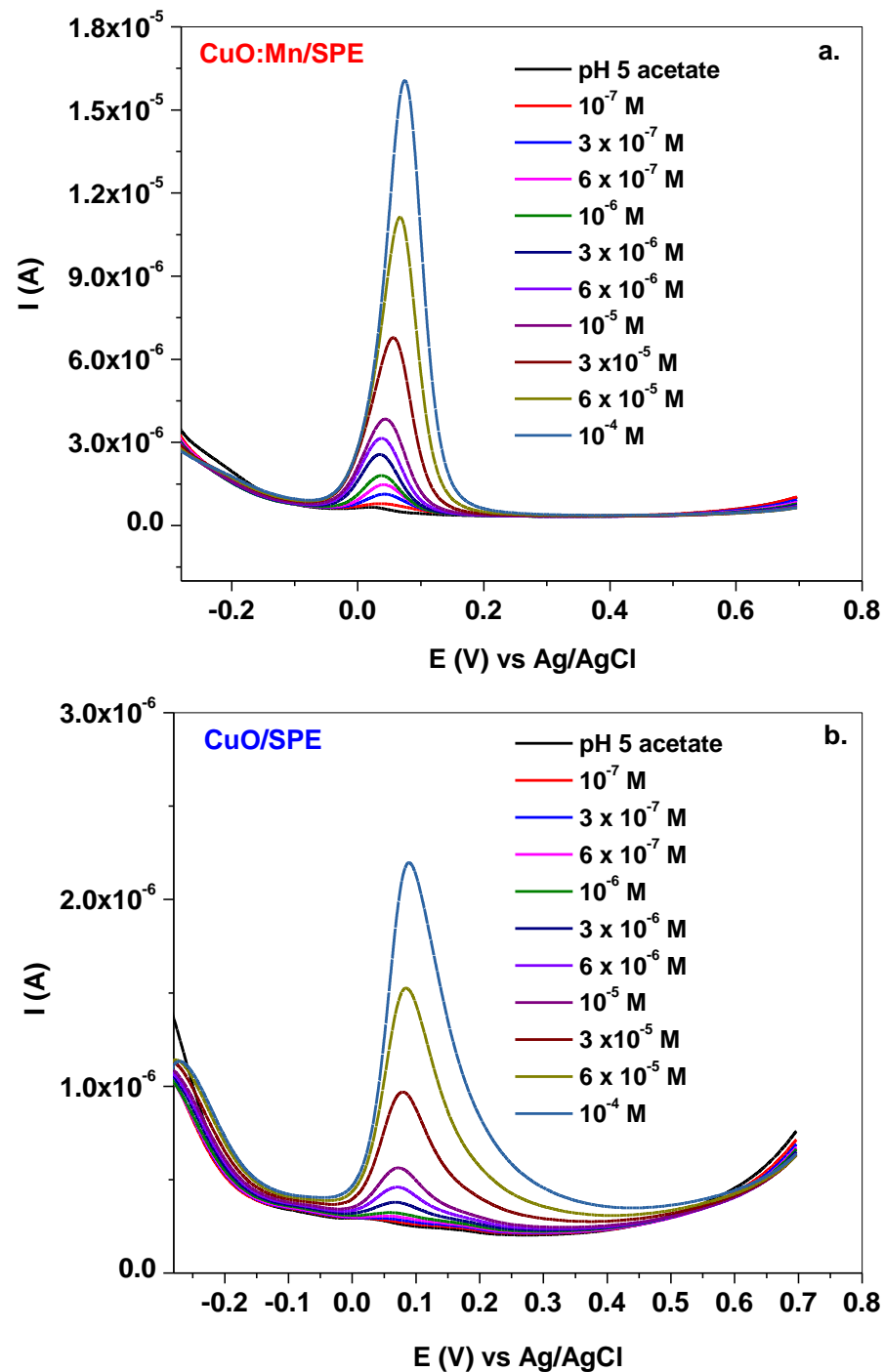


Figure 11. SW voltammograms were recorded with CuO:Mn/SPE (a) and CuO/SPE (b) in solutions containing increasing concentrations of dopamine, 10^{-7} – 10^{-4} M (pH 5.0 acetate buffer); 10 mV/s scan rate.

In the case of bare SPE (green), the linear range is within 3×10^{-7} – 10^{-4} M dopamine ($y = 2.25 \times 10^{-8} + 0.022 \times C$; $R^2 = 0.996$), the LOD is 9.09×10^{-8} M, and the sensitivity is very low, 0.022 A/M. In good agreement with the previous experiments, the performances of CuO/SPE are not significantly improved. Therefore, the linear range is within 10^{-7} – 10^{-4} M dopamine ($y = 1.03 \times 10^{-7} + 0.028 \times C$; $R^2 = 0.99$), the LOD is 3.03×10^{-8} M while the sensitivity is 0.028 A/M. Better results were obtained with CuO:Mn/SPE, where two linear ranges were observed. The first one is within 10^{-7} – 10^{-6} M ($y_1 = 1.95 \times 10^{-7} + 1.09 \times C$; $R^2 = 0.965$) and the second one is within 10^{-6} – 10^{-4} M ($y_2 = 1.63 \times 10^{-6} + 0.14 \times C$;

$R^2 = 0.995$). The LOD is 3.03×10^{-8} M and the sensitivity is extremely high, 1.09 A/M (10^{-7} – 10^{-6} M range). Concerning the second linear range, the sensitivity is also high (0.14 A/M; five times higher than that of bare SPE or CuO/SPE) and the limit of detection is 3.03×10^{-7} M.

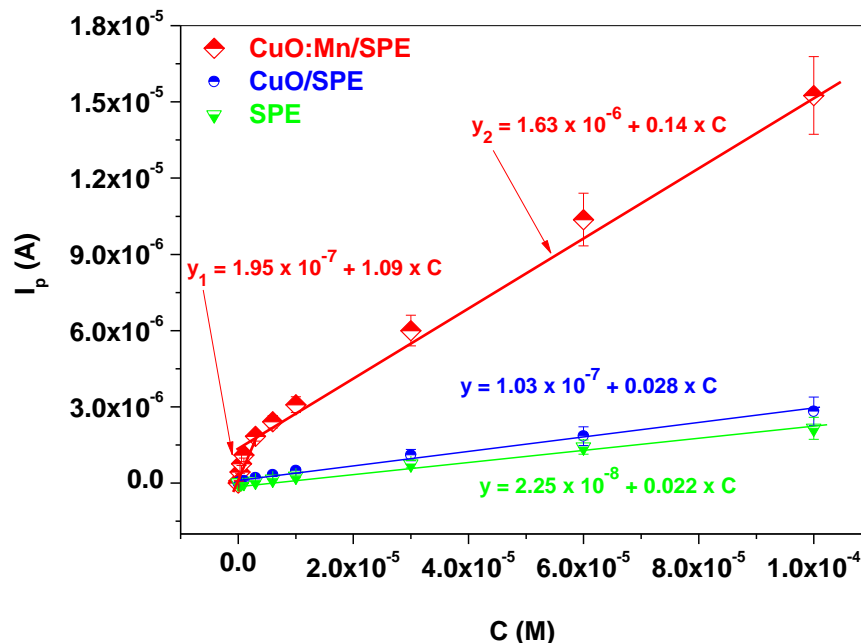


Figure 12. Calibration plots obtained with CuO:Mn/SPE (red; 10^{-7} – 10^{-6} M and 10^{-6} – 10^{-4} M linear ranges); CuO/SPE (blue; 10^{-7} – 10^{-4} M linear range) and bare SPE (green; 3×10^{-7} – 10^{-4} M linear range).

The performances of CuO:Mn/SPE towards dopamine detection were compared with those of other types of electrodes reported in the literature (see Table 1). In most cases the employed electrode has similar or better performances, both in terms of linear range and limit of detection.

Table 1. Assessment of different modified electrodes for measuring dopamine.

Modified Electrode	Linear Range (μ M)	LOD (nM)	Reference
DNA aptamer-GO/nile blue/GCE DNA aptamer-GO/nile blue—reduced graphene oxide/nile blue/gold nanoparticles complex GCE—glassy carbon electrode	0.01–200	1	[74]
Thionin/AuNPs/CNPs/Au Thionin/AuNPs/CNPs—carbon nanoparticles (CNPs) coupled to thionine labeled gold nanoparticles (AuNPs) Au—gold electrode	30–3000	10	[75]
Electrodeposited PEDOT/GO/GCE Electrodeposited PEDOT/GO—nanocomposite composed of conducting polymer poly (3,4-ethylenedioxythiophene) (PEDOT) doped with graphene oxide (GO) GCE—glassy carbon electrode	0.1–175	39	[76]

Table 1. Cont.

Modified Electrode	Linear Range (μM)	LOD (nM)	Reference
GO/PEDOT/GCE GO/PEDOT—nanocomposite of poly(3,4-ethylenedioxythiophene) (PEDOT) doped with GO nanosheets GCE—glassy carbon electrode	1–40	83	[77]
Ag-Pt/pCNFs/GCE Ag-Pt/pCN—Fs—electrospun nanoporous carbon nanofibers (pCNFs) decorated with Ag-Pt bimetallic nanoparticles GCE—glassy carbon electrode	10–500	110	[78]
RGO/Pd-NPs/GCE RGO/Pd-NPs—nanocomposite containing electrochemically reduced graphene oxide (RGO) and palladium nanoparticles (Pd-NPs) GCE—glassy carbon electrode	1–150	233	[79]
Cu₂O/Graphene/GCE Cu ₂ O/graphene—nanocomposites composed of cuprous oxide (Cu ₂ O) and graphene GCE—glassy carbon electrode	0.1–10	10	[80]
GO/SiO₂-MIPs/GCE GO/SiO ₂ -MIPs—composite of SiO ₂ -coated GO and molecularly imprinted polymers γ -methacryloxypropyl trimethoxysilane GCE—glassy carbon electrode	0.05–160	30	[81]
MnO₂ NWs/ERGO/GCE MnO ₂ NWs/ERGO—MnO ₂ nanowires—electrochemically reduced graphene oxide GCE—glassy carbon electrode	0.01–0.10	1	[82]
ZnO/CPE ZnO—zinc oxide nanoparticles CPE—carbon paste electrode	0.1–20	30	[83]
CuO/CPE CuO—copper (II) oxide nanoparticles CPE—carbon paste electrode	0.1–10	10	[54]
3D Pt/RGO/MnO₂/GCE 3D Pt/RGO/MnO ₂ —three dimensional (3D) ternary Pt nanodendrite/reduced graphene oxide/MnO ₂ nanoflower GCE—glassy carbon electrode	1.5–215.56	100	[84]
CuO:Mn/SPE	0.1–1 1–100	30.3	current work

In order to prove the analytical applicability of CuO:Mn/SPE, the electrode was further employed for dopamine quantification in a pharmaceutical drug solution that contained dopamine hydrochloride (5 mg/mL) and different interfering species: sodium metabisulfite (Na₂S₂O₅), maleic acid (C₄H₄O₄), sodium chloride (NaCl), and propylene glycol (C₃H₈O₂). The SW signals were recorded in solution containing the pharmaceutical drug solution (C_x) and in solutions containing C_x and the added volumes (5; 10; 15 μL) of dopamine from the 10⁻³ M stock solution, corresponding to the added C₁, C₂, and C₃

concentrations, respectively (Figure 13a). From the calibration plot (I_p versus the added concentrations— C_{add}), the C_x value was found to be 5.53×10^{-7} M (Figure 13b). By comparing the C_x value with the one calculated from the drug solution (5.24×10^{-7} M), we can conclude that the electrode has excellent ability in the determination of dopamine in the real sample.

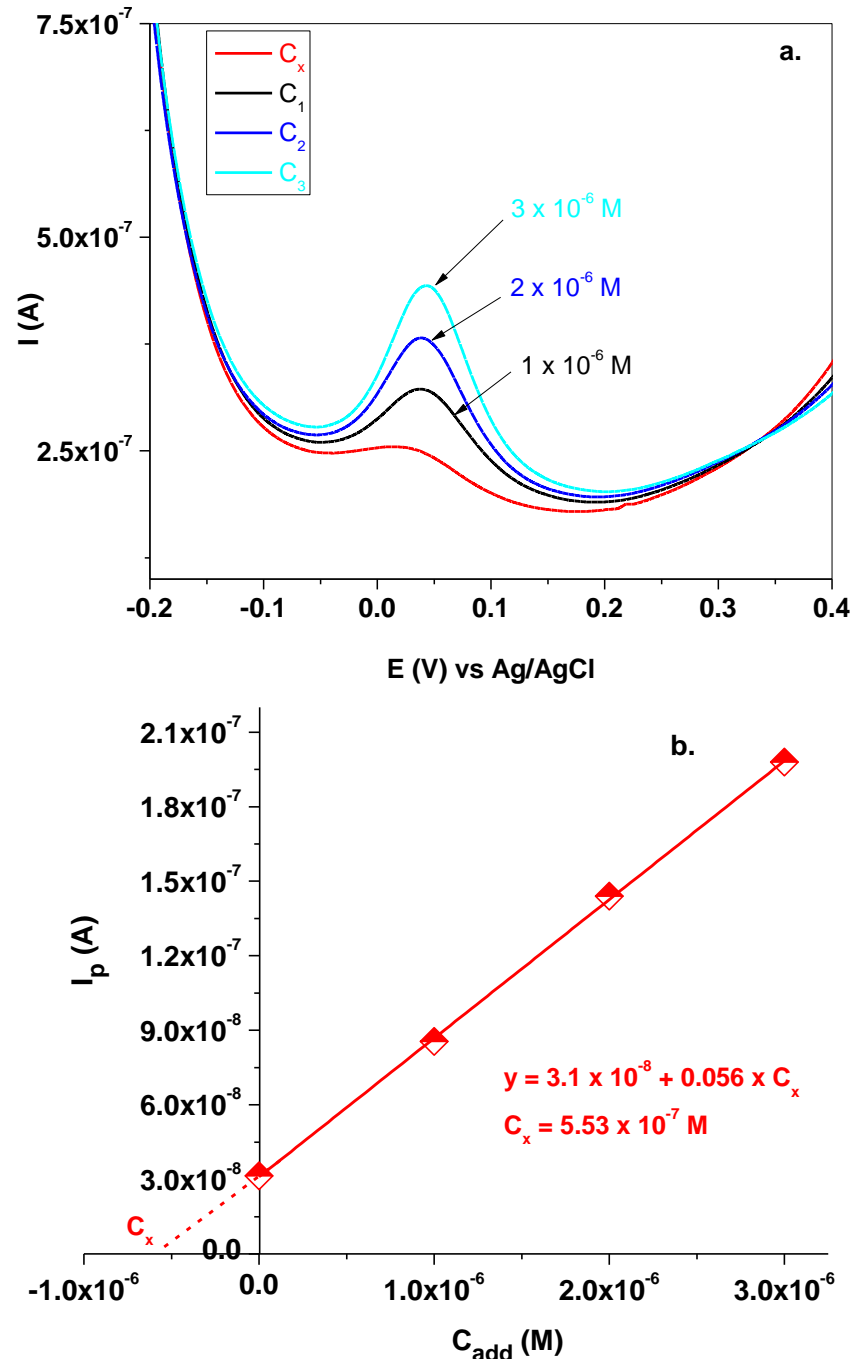


Figure 13. Standard addition method employed for the determination of DA concentration in pharmaceutical drug solution: SW recorded in solutions containing C_x and the added concentrations (C_1 ; C_2 ; C_3) (a); the addition plot used to determine C_x (b).

4. Conclusions

CuO and Mn-doped CuO particles were prepared by the low-cost hydrothermal method using chlorides as precursors. Particles with flat faces and nearly straight edges with the size in the micrometric order were observed by TEM/SEM microscopy. According

to XRD analysis, the CuO crystalline phase was obtained for both samples. The quantitative analysis performed by the XPS technique was used to check the doped sample composition. Thus, 1 at.% manganese doping was confirmed to be in the doped sample, which is in good agreement with the concentration of manganese precursor used in synthesis. The pH effect on the DA oxidation signal for bare and SPE modified electrodes was investigated and determined to be optimum at the value of pH 5.0 (acetate buffer solution). From square wave voltammetry experiments, it was established that CuO:Mn material increased the transfer of electrons between the dopamine molecules and the SPE surface. The electrochemical signal obtained for all electrodes at different dopamine concentrations gave information about the limit of detection and sensitivity. A five times higher sensitivity for CuO:Mn/SPE electrode was reached. The performance of DA detection in real samples of CuO:Mn/SPE was attained on the commercial pharmaceutical drug solution, proving the excellent sensitivity of the doped material.

Supplementary Materials: The following supporting information can be downloaded at: <https://www.mdpi.com/article/10.3390/coatings13061014/s1>, Table S1 Binding energies, line widths raw areas and normalized areas of the quantized core-level XPS lines; Figure S1 Optical images of SPE electrodes; Figure S2 Evolution of the adventitious carbon after consecutive Ar ions etching of sample CuO:Mn; Figure S3 XPS recorded spectrum of Cu 2p core-level of CuO sample together with the corresponding deconvolutions and fitted curves; Figure S4 Survey spectrum of sample CuO. Red bars indicate the expected positions of the most intense Cl core-levels and Auger Cl LMM. These lines were not observed; Figure S5 Cyclic voltammograms recorded with bare SPE with different scanning rates (2–100 mV/s) in solution containing 10^{-3} M potassium hexacyanoferrate (II) and 0.2 M KCl supporting electrolyte (a); the plot of I_{pa} versus the square root of scan rate, $v^{1/2}$ (b); Figure S6 Cyclic voltammograms recorded with CuO:Mn/SPE with different scanning rates (2–100 mV/s) in solution containing 10^{-3} M potassium hexacyanoferrate (II) and 0.2 M KCl supporting electrolyte (a); the plot of I_{pa} versus the square root of scan rate, $v^{1/2}$ (b); Figure S7 The stability of CuO:Mn/SPE, after successive scanning in solution containing 10^{-4} M dopamine (pH 5 acetate); 20 scans with 10 mV/s scan rate; Figure S8 Cyclic voltammograms recorded with CuO:Mn/SPE in solution containing 10^{-4} M dopamine (pH 5.0 acetate buffer), with increasing scan rate: 2–550 mV/s (a); The variation of the current peaks (anodic and cathodic) with the square root of scan rate (b); Figure S9 Equivalent electrical circuit employed to fit the EIS spectra of bare and modified SPE, CuO/SPE and CuO:Mn/SPE; Figure S10. SW voltammograms recorded with bare SPE in solutions containing increasing concentrations of dopamine, 10^{-7} – 10^{-4} M range (pH 5.0 acetate buffer); 10 mV/s scan rate.

Author Contributions: Methodology and samples preparation, S.G. and O.G.; investigation and validation, F.P., L.M. and M.O.M., writing—original draft preparation, supervision, I.-O.P. and S.P. All authors have read and agreed to the published version of the manuscript.

Funding: The authors acknowledge financial support from the Ministry of Research, Innovation and Digitization, CNCS/CCCDI—UEFISCDI, projects number PN-III-P2-2.1-PED-2019-2410 (500PED/2021) and the ‘Nucleu’ Program within the National Plan for Research, Development and Innovation 2022–2027, project number PN 23 24 01 05.

Institutional Review Board Statement: Not applicable.

Informed Consent Statement: Not applicable.

Data Availability Statement: Data will be provided upon reasonable request to the corresponding author.

Acknowledgments: The authors are grateful to Ana Maria Raluca Gherman for recording TEM and SEM micrographs for CuO and CuO:Mn materials.

Conflicts of Interest: The authors declare no conflict of interest.

References

1. Channer, B.; Matt, S.M.; Nickoloff-Bybel, E.A.; Pappa, V.; Agarwal, Y.; Wickman, J.; Gaskill, P.J. Dopamine, Immunity and Disease. *Pharmacol. Rev.* **2023**, *75*, 618. [[CrossRef](#)] [[PubMed](#)]
2. Bove, C.; Anselmi, L.; Travagli, R.A. Altered gastric tone and motility response to brain-stem dopamine in a rat model of parkinsonism. *Am. J. Physiol. Gastrointest. Liver. Physiol.* **2019**, *317*, G1–G7. [[CrossRef](#)] [[PubMed](#)]
3. Bucolo, C.; Leggio, G.M.; Drago, F.; Salomone, S. Dopamine outside the brain: The eye, cardiovascular system and endocrine pancreas. *Pharmacol. Ther.* **2019**, *203*, 107392. [[CrossRef](#)] [[PubMed](#)]
4. Tavares, G.; Martins, F.O.; Melo, B.F.; Matafome, P.; Conde, S.V. Peripheral Dopamine Directly Acts on Insulin-Sensitive Tissues to Regulate Insulin Signaling and Metabolic Function. *Front. Pharmacol.* **2021**, *12*, 713418. [[CrossRef](#)]
5. Hou, S.; Kasner, M.L.; Su, S.; Patel, K.; Cuellari, R. Highly Sensitive and Selective Dopamine Biosensor Fabricated with Silanized Graphene. *J. Phys. Chem. C* **2010**, *114*, 14915–14921. [[CrossRef](#)]
6. Dickson, D.W. Neuropathology of Parkinson disease. *Parkinsonism Relat. Disord.* **2018**, *46* (Suppl. 1), S30–S33. [[CrossRef](#)]
7. Neumann, J.; Hofmann, B.; Dhein, S.; Gergs, U. Role of Dopamine in the Heart in Health and Disease. *Int. J. Mol. Sci.* **2023**, *24*, 5042. [[CrossRef](#)]
8. Klein, M.O.; Battagello, D.S.; Cardoso, A.R.; Hauser, D.N.; Bittencourt, J.C.; Correa, R.G. Dopamine: Functions, Signaling, and Association with Neurological Diseases. *Cell. Mol. Neurobiol.* **2019**, *39*, 31–59. [[CrossRef](#)]
9. Vázquez-González, D.; Carreón-Trujillo, S.; Alvarez-Arellano, L.; Abarca-Merlin, D.M.; Domínguez-López, P.; Salazar-García, M.; Corona, J.C. A Potential Role for Neuroinflammation in ADHD. *Adv. Exp. Med. Biol.* **2023**, *1411*, 327–356. [[CrossRef](#)]
10. Namkung, S.M.; Choi, J.S.; Park, J.H.; Yang, M.G.; Lee, M.W.; Kim, S.W. Detection of dopamine and serotonin by competitive enzyme-linked immunosorbent assay. *Kor. J. Clin. Lab. Sci.* **2017**, *49*, 220–226. [[CrossRef](#)]
11. Zhao, H.-X.; Mu, H.; Bai, Y.-H.; Yu, H.; Hu, Y.-M. A rapid method for the determination of dopamine in porcine muscle by pre-column derivatization and HPLC with fluorescence detection. *J. Pharmaceut. Anal.* **2011**, *1*, 208–212. [[CrossRef](#)] [[PubMed](#)]
12. Perez-Fernandez, V.; Harman, D.G.; Morley, J.W.; Cameron, M.A. Optimized Method to Quantify Dopamine Turnover in the Mammalian Retina. *Anal. Chem.* **2017**, *89*, 12276–12283. [[CrossRef](#)] [[PubMed](#)]
13. Barreto, W.; Barreto, S.; Ando, R.; Santos, P.; DiMauro, E.; Jorge, T.; Raman, I.R. UV-vis and EPR characterization of two copper dioxolene complexes derived from L-dopa and dopamine. *Spectrochim. Acta* **2008**, *71*, 1419–1424. [[CrossRef](#)]
14. Khattar, R.; Mathur, P. 1-(Pyridin-2-ylmethyl)-2-(3-(1-(pyridin-2-ylmethyl)benzimidazol-2-yl) propyl) benzimidazole and its copper(II) complex as a new fluorescent sensor for dopamine (4-(2-aminoethyl)benzene-1,2-diol). *Inorg. Chem. Commun.* **2013**, *31*, 37–43. [[CrossRef](#)]
15. Li, H.; Li, C.; Yan, Z.; Yang, J.; Chen, H. Simultaneous monitoring multiple neurotransmitters and neuromodulators during cerebral ischemia/reperfusion in rats by microdialysis and capillary electrophoresis. *J. Neurosci. Methods* **2010**, *189*, 162–168. [[CrossRef](#)]
16. Lakard, S.; Pavel, I.A.; Lakard, B. Electrochemical Biosensing of Dopamine Neurotransmitter: A Review. *Biosensors* **2021**, *11*, 179. [[CrossRef](#)]
17. Magerusan, L.; Pogacean, F.; Pruneanu, S. Enhanced Acetaminophen Electrochemical Sensing Based on Nitrogen-Doped Graphene. *Int. J. Mol. Sci.* **2022**, *23*, 14866. [[CrossRef](#)]
18. Tang, Z.D.; Jiang, K.; Sun, S.; Qian, S.H.; Wang, Y.H.; Lin, H.W. A conjugated carbon-dot-tyrosinase bioprobe for highly selective and sensitive detection of dopamine. *Analyst* **2019**, *144*, 468–473. [[CrossRef](#)]
19. Li, Z.K.; Zheng, Y.J.; Gao, T.T.; Liu, H.; Zhang, J.; Zhou, G.W. Fabrication of biosensor based on core-shell and large void structured magnetic mesoporous microspheres immobilized with laccase for dopamine detection. *J. Mater. Sci.* **2018**, *53*, 7996–8008. [[CrossRef](#)]
20. Florescu, M.; David, M. Tyrosinase-Based Biosensors for Selective Dopamine Detection. *Sensors* **2017**, *17*, 1314. [[CrossRef](#)]
21. Koh, D.Y.; Kook, J.K.; Lee, S.W. Highly fluorescent oligodopamine (F-ODA) for accurate and sensitive detection of the neurotransmitter dopamine. *Anal. Biochem.* **2020**, *591*, 113571. [[CrossRef](#)] [[PubMed](#)]
22. Armengaud, C.; Moisy, P.; Bedioui, F.; Devynck, J. Electrochemistry of conducting polypyrrole films containing cobalt porphyrin. *J. Electroanal. Chem.* **1990**, *277*, 197–211. [[CrossRef](#)]
23. Li, X.-B.; Rahman, M.M.; Xu, G.-R.; Lee, J.-J. Highly Sensitive and Selective Detection of Dopamine at Poly(chromotrope 2B)-Modified Glassy Carbon Electrode in the Presence of Uric Acid and Ascorbic Acid. *Electrochim. Acta* **2015**, *173*, 440–447. [[CrossRef](#)]
24. Uge, A.; Zeybek, D.K.; Zeybek, B. An electrochemical sensor for sensitive detection of dopamine based on MWCNTs/CeO₂-PEDOT composite. *J. Electroanal. Chem.* **2018**, *813*, 134–142. [[CrossRef](#)]
25. Bae, S.R.; Jeong, H.S.; Jo, S.H.; Jeon, S.W. The determination of dopamine in the presence of ascorbic acid at the modified glassy carbon electrode with phytic acid and single-walled carbon nanotubes. *Bull. Korean Chem. Soc.* **2007**, *28*, 2363–2368. [[CrossRef](#)]
26. Zhang, X.J.; Zheng, J.B. High-index {hk0} facets platinum concave nanocubes loaded on multiwall carbon nanotubes and graphene oxide nanocomposite for highly sensitive simultaneous detection of dopamine and uric acid. *Talanta* **2020**, *207*, 120296. [[CrossRef](#)]
27. Guo, X.; Yue, H.; Song, S.; Huang, S.; Gao, X.; Chen, H.; Wu, P.; Zhang, T.; Wang, Z. Simultaneous electrochemical determination of dopamine and uric acid based on MoS₂ nanoflowers-graphene/ITO electrode. *Microchem. J.* **2020**, *154*, 104527. [[CrossRef](#)]
28. Yu, G.; Xia, J.; Zhang, F.; Wang, Z. Hierarchical and hybrid RGO/ZIF-8 nanocomposite as electrochemical sensor for ultrasensitive determination of dopamine. *J. Electroanal. Chem.* **2017**, *801*, 496–502. [[CrossRef](#)]

29. Kim, D.S.; Kang, E.S.; Baek, S.; Choo, S.-S.; Chung, Y.-H.; Lee, D.; Min, Y.; Kim, T.-H. Electrochemical detection of dopamine using periodic cylindrical gold nanoelectrode arrays. *Sci. Rep.* **2018**, *8*, 14049. [[CrossRef](#)]
30. Fredj, Z.; Sawan, M. Advanced Nanomaterials-Based Electrochemical Biosensors for Catecholamines Detection: Challenges and Trends. *Biosensors* **2023**, *13*, 211. [[CrossRef](#)]
31. Decarli, N.O.; Zapp, E.; Silveira de Souza, B.; Santana, E.R.; Winiarski, J.P.; Cruz Vieira, I. Biosensor based on laccase-halloysite nanotube and imidazolium zwitterionic surfactant for dopamine determination. *Biochem. Eng. J.* **2022**, *186*, 108565. [[CrossRef](#)]
32. Pimpilova, M.; Kamarska, K.; Dimcheva, N. Biosensing Dopamine and L-Epinephrine with Laccase (*Trametes pubescens*) Immobilized on a Gold Modified Electrode. *Biosensors* **2022**, *12*, 719. [[CrossRef](#)]
33. Álvarez-Martos, I.; Ferapontova, E.E. Electrochemical Label-Free Aptasensor for Specific Analysis of Dopamine in Serum in the Presence of Structurally Related Neurotransmitters. *Anal. Chem.* **2016**, *88*, 3608–3616. [[CrossRef](#)] [[PubMed](#)]
34. Molinnus, D.; Hardt, G.; Käver, L.; Willenberg, H.S.; Poghossian, A.; Keusgen, M.; Schöning, M.J. Detection of Adrenaline Based on Bioelectrocatalytical System to Support Tumor Diagnostic Technology. *Proceedings* **2017**, *1*, 506. [[CrossRef](#)]
35. Josypčuk, O.; Berek, J.; Josypčuk, B. Amperometric Determination of Catecholamines by Enzymatic Biosensors in Flow Systems. *Electroanalysis* **2018**, *30*, 1163–1171. [[CrossRef](#)]
36. Winiarski, J.P.; Ferreira Tavares, B.; De Fátima Ulbrich, K.; De Campos, C.E.M.; Souza, A.A.U.; Guelli, U.; Souza, S.M.A.; Jost, C.L. Development of a multianalyte electrochemical sensor for depression biomarkers based on a waste of the steel industry for a sustainable and one-step electrode modification. *Microchem. J.* **2022**, *175*, 107141. [[CrossRef](#)]
37. Yang, W.; Yu, Y.; Tang, Y.; Li, K.; Zhao, Z.; Li, M.; Yin, G.; Li, H.; Sun, S. Enhancing electrochemical detection of dopamine via dumbbell-like FePt-Fe₃O₄ nanoparticles. *Nanoscale* **2017**, *9*, 1022–1027. [[CrossRef](#)] [[PubMed](#)]
38. Huang, Y.; Zhang, Y.; Liu, D.; Li, M.; Yu, Y.; Yang, W.; Li, H. Facile synthesis of highly ordered mesoporous Fe₃O₄ with ultrasensitive detection of dopamine. *Talanta* **2019**, *201*, 511–518. [[CrossRef](#)]
39. Huang, Y.; Tang, Y.; Xu, S.; Feng, M.; Yu, Y.; Yang, W.; Li, H. A highly sensitive sensor based on ordered mesoporous ZnFe₂O₄ for electrochemical detection of dopamine. *Anal. Chim. Acta.* **2020**, *1096*, 26–33. [[CrossRef](#)]
40. Fernandes, D.M.; Costa, M.; Pereira, C.; Bachiller-Baeza, B.; Rodríguez-Ramos, I.; Guerrero-Ruiz, A.; Freire, C. Novel electrochemical sensor based on N-doped carbon nanotubes and Fe₃O₄ nanoparticles: Simultaneous voltammetric determination of ascorbic acid, dopamine and uric acid. *J. Colloid Interface Sci.* **2014**, *432*, 207–213. [[CrossRef](#)]
41. Sato, N.; Haruta, M.; Ohta, Y.; Sasagawa, K.; Ohta, J.; Pewnim, N.; Jongprateep, O. Fe₂O₃/MWCNTs modified microdialysis electrode for dopamine detection. *Mater. Res. Express* **2020**, *7*, 015701. [[CrossRef](#)]
42. Intan, R.S.; Novi, A.; Tae, K.H. Nanomaterial-modified Hybrid Platforms for Precise Electrochemical Detection of Dopamine. *BioChip J.* **2019**, *13*, 20–29. [[CrossRef](#)]
43. Swamy, B.K.; Shiprath, K.; Ratnam, K.V.; Manjunatha, H.; Janardan, S.; Ratnamala, A.; Babu Naidu, K.C.; Ramesh, S.; Suresh Babu, K. Electrochemical Detection of Dopamine and Tyrosine using Metal oxide (MO, M=Cu and Ni) Modified Graphite Electrode: A Comparative Study. *Biointerface Res. Appl. Chem.* **2020**, *10*, 6460–6473. [[CrossRef](#)]
44. Zhang, H.; Zhu, Q.; Zhang, Y. One-pot synthesis and hierarchical assembly of hollow Cu₂O microspheres with nanocrystals-composed porous multishell and their gas-sensing properties. *Adv. Funct. Mater.* **2007**, *17*, 2766–2771. [[CrossRef](#)]
45. Zhang, J.; Liu, J.; Peng, Q. Nearly monodisperse Cu₂O and CuO nanospheres: Preparation and applications for sensitive gas sensors. *Chem. Mater.* **2006**, *18*, 867–871. [[CrossRef](#)]
46. Xu, F.; Deng, M.; Li, G.; Chen, S.; Wang, L. Electrochemical behavior of cuprous oxide—Reduced graphene oxide nanocomposite and their application in nonenzymatic hydrogen peroxide sensing. *Electrochim. Acta* **2013**, *88*, 59–65. [[CrossRef](#)]
47. Miao, X.M.; Yuan, R.; Chai, Y.Q.; Shi, Y.T.; Yuan, Y.Y. Direct electrocatalytic reduction of hydrogen peroxide on Nafion and copper oxide nanoparticles modified Pt electrode. *J. Electroanal. Chem.* **2008**, *612*, 157–163. [[CrossRef](#)]
48. Song, H.; Ni, Y.; Kokot, S. A novel electrochemical sensor based on the copper-doped copper oxide nano-particles for the analysis of hydrogen peroxide. *Colloids Surf. A Eng. Asp.* **2015**, *465*, 153–158. [[CrossRef](#)]
49. He, G.-W.; Jiang, J.-Q.; Wu, D.; You, Y.-L.; Yang, X.; Wu, F.; Hu, Y.-J. A novel nonenzymatic hydrogen peroxide electrochemical sensor based on facile synthesis of copper oxide nanoparticles doping into graphene sheets @ cerium oxide nanocomposites sensitized screen printed electrode. *Int. J. Electrochem. Sci.* **2016**, *11*, 8486–8498. [[CrossRef](#)]
50. Alizadeh, T.; Mirzagholipour, S. Anafion-free non-enzymatic amperometric glucose sensor based on copper oxide nanoparticles—Graphene nanocomposite. *Sens. Actuators B Chem.* **2014**, *198*, 438–477. [[CrossRef](#)]
51. Dhara, K.; Thiagarajan, R.; Nair, B.G. Highly sensitive and wide-range nonenzymatic disposable glucose sensor based on a screen printed carbon electrode modified with reduced graphene oxide and Pd-CuO nanoparticles. *Microchim. Acta* **2015**, *182*, 2183–2192. [[CrossRef](#)]
52. Yan, X.; Yang, J.; Ma, L.; Tong, X.; Wang, Y.; Jin, G.; Guo, X.Y. Size-controlled synthesis of Cu₂O nanoparticles on reduced graphene oxide sheets and their application as non-enzymatic glucose sensor materials. *J. Solid State Electrochem.* **2015**, *19*, 3195–3199. [[CrossRef](#)]
53. Harris, P.A.; Taylor, R.; Minor, B.L.; Elliott, V.; Fernandez, M.; O’Neal, L.; McLeod, L.; Delacqua, G.; Delacqua, F.; Kirby, J.; et al. Highly selective and sensitive determination of dopamine by the novel molecularly imprinted poly (nicotinamide)/CuO nanoparticles modified electrode. *Biosens. Bioelectron.* **2015**, *67*, 121–128. [[CrossRef](#)]
54. Reddy, S.; Swamy, B.E.K.; Jayadevappa, H. CuO nanoparticle sensor for the electrochemical determination of dopamine. *Electrochim. Acta* **2012**, *61*, 78–86. [[CrossRef](#)]

55. Li, H.; Ye, L.; Wang, Y.; Xie, C. A glassy carbon electrode modified with hollow cubic cuprous oxide for voltammetric sensing of L-cysteine. *Microchim. Acta* **2018**, *185*, 5. [[CrossRef](#)]
56. Gu, W.; Wang, M.; Mao, X.; Wang, Y.; Li, L.; Xia, W. A facile sensitive L-tyrosine electrochemical sensor based on coupled CuO/Cu₂O nanoparticles and multi-walled carbon nanotubes nanocomposite film. *Anal. Methods* **2015**, *7*, 1313–1320. [[CrossRef](#)]
57. Zhou, S.; Wei, D.; Shi, H.; Feng, X.; Xue, K.; Zhang, F.; Song, W. Sodium dodecyl benzene sulfonate functionalized graphene for confined electrochemical growth of metal/oxide nanocomposites for sensing application. *Talanta* **2013**, *107*, 349–355. [[CrossRef](#)] [[PubMed](#)]
58. Khoshhesab, Z.M. Simultaneous electrochemical determination of acetaminophen, caffeine and ascorbic acid using a new electrochemical sensor based on CuO-graphene nanocomposite. *RSC. Adv.* **2015**, *5*, 95140–95148. [[CrossRef](#)]
59. Pana, O.; Leostean, C.; Soran, M.L.; Stefan, M.; Macavei, S.; Gutoiu, S.; Pop, V.; Chauvet, O. Synthesis and characterization of Fe-Pt based multi-shell magnetic nanoparticles. *J. Alloy. Comp.* **2013**, *574*, 477–485. [[CrossRef](#)]
60. Macavei, S.; Toloman, D.; Stefan, M.; Popa, A.; Barbu-Tudoran, L.; Grosan, L.; Suci, R.; Pana, O.; Balan, R. Characterization of Cu₂ZnSnS₄ Thin Film Deposited by Pulse Laser Deposition. In Proceedings of the 11th International Conference of Processes In Isotopes and Molecules, Cluj-Napoca, Romania, 27–29 September 2017; Volume 1917, p. 040010. [[CrossRef](#)]
61. Stefan, M.; Pana, O.; Leostean, C.; Popa, A.; Toloman, D.; Macavei, S.; Lazar, D.; Barbu-Tudoran, L. Morpho-structural and photocatalytic properties of SnO₂ nanoparticles. *Stud. UBB Chem.* **2019**, *3*, 99–109. [[CrossRef](#)]
62. Sonia, S.; Jose Annsi, I.; Kumar, P.S.; Mangalaraj, D.; Viswanathan, C.; Ponpandian, N. Hydrothermal synthesis of novel Zn doped CuO nanoflowers as an efficient photodegradation material for textile dyes. *Mater Lett.* **2015**, *144*, 127–130. [[CrossRef](#)]
63. Yildiz, A.; Horzum, S.; Serin, N.; Serin, T. Hopping conduction in In-doped CuO thin films. *Appl. Surf. Sci.* **2014**, *318*, 105–107. [[CrossRef](#)]
64. Gao, W.L.; Yang, S.H.; Yang, S.g.; Lv, L.Y.; Du, Y.W. Synthesis and magnetic properties of Mn doped CuO. *Phys. Lett. A* **2010**, *375*, 180–182. [[CrossRef](#)]
65. Mahomed Basith, N.; Judith Vijaya, J.; John Kennedy, L.; Bououdina, M. Structural, optical and room temperature ferromagnetic properties of Fe-doped CuO nanostructures. *Phys. E Low-Dimens. Syst. Nanostructures* **2013**, *53*, 193–199. [[CrossRef](#)]
66. Mahomed Basith, N.; Judith Vijaya, J.; John Kennedy, L.; Bououdina, M. Structural, morphological, optical, and magnetic properties of Ni-doped CuO nanostructures prepared by rapid microwave combustion method. *Mater. Sci. Semicond. Process.* **2014**, *17*, 110–118. [[CrossRef](#)]
67. Khalid, A.; Ahmad, P.; Alharthi, A.I.; Muhammad, S.; Khandaker, M.U.; Rehman, M.; Faruque, M.R.I.; Din, I.U.; Alotaibi, M.A.; Alzimami, K.; et al. Structural, Optical, and Antibacterial Efficacy of Pure and Zinc-Doped Copper Oxide Against Pathogenic Bacteria. *Nanomaterials* **2021**, *11*, 451. [[CrossRef](#)]
68. Popa, A.; Stefan, M.; Toloman, D.; Pana, O.; Mesaros, A.; Leostean, C.; Macavei, S.; Marincas, O.; Suci, R.; Barbu-Tudoran, L. Fe₃O₄-TiO₂: Gd nanoparticles with enhanced photocatalytic activity and magnetic recyclability. *Powder Technol.* **2018**, *325*, 441–451. [[CrossRef](#)]
69. Biesinger, M.C. Advanced analysis of copper X-ray photoelectron spectra. *Surf. Interface Anal.* **2017**, *49*, 1325–1334. [[CrossRef](#)]
70. Chawla, S.K.; Sankarraman, N.; Payer, J.H. Diagnostic spectra for XPS analysis of Cu-O-S-H compounds. *J. Electron Spectrosc. Relat. Phenom.* **1992**, *61*, 1–18. [[CrossRef](#)]
71. Ghijsen, J.; Tjeng, L.H.; Van Elp, J.; Eskes, H.; Westerink, J.; Sawatzky, G.A. Electronic structure of Cu₂O and CuO. *Phys. Rev. B* **1988**, *38*, 11322–11330. [[CrossRef](#)]
72. Svintsitskiy, D.A.; Kardash, T.Y.; Stonkus, O.A.; Slavinskaya, E.M.; Stadnichenko, A.I.; Koscheev, S.V.; Chupakhin, A.P.; Boronin, A.I. In Situ XRD, XPS, TEM, and TPR Study of Highly Active in CO Oxidation CuO Nanopowders. *J. Phys. Chem. C* **2013**, *117*, 14588–14599. [[CrossRef](#)]
73. Piero, Z. *Inorganic Electrochemistry Theory, Practice and Application*; Royal Society of Chemistry: London, UK, 2003.
74. Jin, H.; Zhao, C.Q.; Gui, R.J.; Gao, X.H.; Wang, Z.H. Reduced graphene oxide/nile blue/gold nanoparticles complex-modified glassy carbon electrode used as a sensitive and label-free aptasensor for ratiometric electrochemical sensing of dopamine. *Anal. Chim. Acta.* **2018**, *1025*, 154–162. [[CrossRef](#)]
75. Xu, Y.Q.; Hun, X.; Liu, F.; Wen, X.L.; Luo, X.L. Aptamer biosensor for dopamine based on a gold electrode modified with carbon nanoparticles and thionine labeled gold nanoparticles as probe. *Microchim. Acta* **2015**, *182*, 1797–1802. [[CrossRef](#)]
76. Wang, W.; Xu, G.; Cui, X.T.; Sheng, G.; Luo, X. Enhanced catalytic and dopamine sensing properties of electrochemically reduced conducting polymer nanocomposite doped with pure graphene oxide. *Biosens. Bioelectron.* **2014**, *58*, 153–156. [[CrossRef](#)]
77. Weaver, C.L.; Li, H.; Luo, X.; Cui, X.T. A graphene oxide/conducting polymer nanocomposite for electrochemical dopamine detection: Origin of improved sensitivity and specificity. *J. Mater. Chem. B* **2014**, *2*, 5209–5219. [[CrossRef](#)]
78. Huang, Y.; Miao, Y.E.; Ji, S.; Tjiu, W.W.; Liu, T. Electrospun carbon nanofibers decorated with Ag-Pt bimetallic nanoparticles for selective detection of dopamine. *ACS Appl. Mater. Interfaces* **2014**, *6*, 12449–12456. [[CrossRef](#)] [[PubMed](#)]
79. Palanisamy, S.; Ku, S.H.; Chen, S.M. Dopamine Sensor Based on a Glassy Carbon Electrode Modified with a Reduced Graphene Oxide and Palladium Nanoparticles Composite. *Microchim. Acta* **2013**, *180*, 1037–1042. [[CrossRef](#)]
80. Zhang, F.; Li, Y.; Gu, Y.; Wang, Z.; Wang, C. One-pot solvothermal synthesis of a Cu₂O/graphene nanocomposite and its application in an electrochemical sensor for dopamine. *Microchim. Acta* **2011**, *173*, 103–109. [[CrossRef](#)]
81. Zeng, Y.; Zhou, Y.; Kong, L.; Zhou, T.; Shi, G. A novel composite of SiO₂-coated graphene oxide and molecularly imprinted polymers for electrochemical sensing dopamine. *Biosens. Bioelectron.* **2013**, *45*, 25–33. [[CrossRef](#)] [[PubMed](#)]

82. He, Q.; Liu, J.; Liu, X.; Li, G.; Chen, D.; Deng, P.; Liang, J. A Promising Sensing Platform toward Dopamine Using MnO₂ Nanowires/Electro-Reduced Graphene Oxide Composites. *Electrochim. Acta* **2019**, *296*, 683–692. [[CrossRef](#)]
83. Reddy, S.; Swamy, B.E.K.; Chandrashekar, B.N.; Chitravathi, S.; Jayadevappa, H. Cationic surfactants–assisted synthesis of ZnO nanoparticles and their modified carbon paste electrode for electrochemical investigation of dopamine. *Anal. Bioanal. Electrochem.* **2012**, *4*, 186–196.
84. Yang, B.; Wang, J.; Duan, B.; Zhu, M.; Yang, P.; Du, Y. A three dimensional Pt nanodendrite/graphene/MnO₂ nanoflower modified electrode for the sensitive and selective detection of dopamine. *J. Mater. Chem. B* **2015**, *3*, 7440–7448. [[CrossRef](#)] [[PubMed](#)]

Disclaimer/Publisher’s Note: The statements, opinions and data contained in all publications are solely those of the individual author(s) and contributor(s) and not of MDPI and/or the editor(s). MDPI and/or the editor(s) disclaim responsibility for any injury to people or property resulting from any ideas, methods, instructions or products referred to in the content.